Activated Carbon Adsorption and Desorption of Toluene in the Aqueous Phase

Dimitrios Chatzopoulos and Arvind Varma
Dept. of Chemical Engineering

Robert L. Irvine
Dept. of Civil Engineering and Geological Sciences
Center for Bioengineering and Pollution Control

University of Notre Dame, Notre Dame, IN 46556

The equilibrium and dynamics of toluene adsorption and desorption in single-component aqueous solutions were investigated. Adsorption rates in a batch reactor under a variety of operating conditions were fitted successfully with the homogeneous surface diffusion model and a surface diffusion coefficient that increases exponentially with surface concentration. The dependence of the external mass-transfer coefficient on the hydrodynamic conditions in the liquid phase was taken into account. Desorption studies in the aqueous phase and solvent regeneration of toluene-loaded activated carbon suggest that only a small fraction of toluene adsorbs irreversibly. Moreover, irreversible adsorption occurs only on virgin activated carbon, while adsorption on solvent-regenerated activated carbon is fully reversible. After accounting for irreversible adsorption, the model successfully predicted toluene desorption rates in the aqueous phase under various operating conditions using toluene transport parameters determined from the adsorption studies.

Introduction

Adsorption on activated carbon is one of the most effective and dependable technologies currently available for the treatment of drinking water and wastewaters contaminated with low concentrations of hazardous compounds. In order to effectively design activated carbon adsorption units and to develop mathematical models that can successfully describe their operation, information on both the adsorption and the desorption of individual pollutants is required. While extensive experimental and modeling studies have been reported to date on the activated carbon adsorption of a broad spectrum of hazardous compounds from aqueous solutions (cf. Crittenden et al., 1987; Noll et al., 1992), relatively little attention has been paid to the desorption of these compounds. However, reliable information on the degree of adsorption irreversibility for these compounds and on the dynamics of their desorption in the aqueous phase could significantly enhance our ability to describe adsorption equilibrium and rates in multicomponent systems, as well as the chromatographic displacement commonly observed in the treatment of real wastewaters due to their time-varying composition. Moreover, successful prediction of the dynamics of both adsorption and desorption would facilitate the development of novel applications such as the design of hybrid systems which combine biological degradation and activated carbon adsorption treatment (cf. Chozick and Irvine, 1991), as well as the evaluation of the feasibility of biological regeneration as a method for recovering the adsorptive capacity of spent activated carbon (cf. Hutchinson and Robinson, 1990) in order to substantially decrease the cost associated with the operation of the adsorption unit.

This study addresses the adsorption and desorption of toluene, a volatile organic compound commonly found in industrial wastewaters (for example, from the paint industry) and in groundwaters contaminated from leaking gasoline storage tanks, on activated carbon. Results from both equilibrium and batch rate adsorption and desorption studies in aqueous solutions are given. A model that considers external mass transfer and surface diffusion inside the activated carbon is used to describe the adsorption and desorption dynamics.

Correspondence concerning this article should be addressed to A. Varma.

Previous adsorption studies

A large number of experimental and modeling studies on the adsorption of organics from aqueous solutions on activated carbon have previously been reported. Despite the fact that activated carbon contains a wide range of pore sizes (cf. Famularo et al., 1980; Peel et al., 1981), adsorption rates in most modeling studies have been described using the "homogeneous" particle models which assume isotropic adsorbent particles with a narrow pore-size distribution (cf. Fritz et al., 1981; Hand et al., 1983). This is primarily because of the small number of solute transport parameters involved and the low computational effort required for the solution of these models. Although earlier models (cf. Furusawa and Smith, 1974) considered intraparticle solute diffusion to take place only in the fluid contained in the pores (that is, pore diffusion), a number of studies have clearly demonstrated that the dominant mechanism of intraparticle solute transport for activated carbon adsorption of organics from aqueous solutions is surface diffusion (cf. Neretnieks, 1976; Fritz et al., 1981; Hand et al., 1983).

Currently, activated carbon adsorption from aqueous solutions is most commonly described by use of the homogeneous surface diffusion model (HSDM) (or solid diffusion model) (cf. Hand et al., 1983; Al-Duri and McKay, 1991). In most cases, the surface diffusion coefficient D_s is assumed to remain constant throughout the adsorption process (cf. Fritz et al., 1981; Hand et al., 1983). However, there has been considerable evidence that D_s increases with surface loading both in single-component and in multicomponent solutions (cf. Sudo et al., 1978; Al-Duri and McKay, 1991). This phenomenon has been well-established for the diffusion of gases on solid surfaces and can be explained by the energetic heterogeneity of the surface, the increase in the mean free path of surface diffusion with surface loading and the lateral interactions among the adsorbed molecules at high surface coverages (cf. Sudo et al., 1978; Kapoor et al., 1989). In addition, a $D_s(q)$ dependence also arises when the solute diffusion flux is represented in terms of the concentration gradient rather than the chemical potential gradient on the surface (cf. Sudo et al., 1978; Ruthven, 1984).

A review of existing models for the concentration dependence of the surface diffusion coefficient D_s in gas-solid systems has been presented recently by Kapoor et al. (1989). Among these models, the one proposed by Gilliland et al. (1974) has also been widely used to describe the dynamics of adsorption from dilute aqueous solutions (cf. Neretnieks, 1976; Muraki et al., 1982; Seidel and Carl, 1989):

$$D_s = D_{so} \exp\left(\frac{-\alpha \Delta H_{st}}{R_g T}\right) \tag{1}$$

where α is an experimentally determined constant whose value depends on the dominant type of bonds between the surface and the adsorbate (Kapoor et al., 1989). Equation 1 expresses the dependence of D_s on the surface concentration q implicitly through the variation of the isosteric heat of adsorption ΔH_{st} with surface concentration. Although this variation can be measured experimentally (cf. Sladek et al., 1974; Okazaki et al., 1981), the need for experimental studies has often been overcome by either arbitrarily assuming a $\Delta H_{st}(q)$ variation (Neretnieks, 1976) or by adopting the $\Delta H_{st}(q)$ distribution implied by the adsorption isotherm used (Muraki et al., 1982; Suzuki and Fujii, 1982; Itaya et al., 1987; Seidel and Carl, 1989).

Among others, Neretnieks (1976), Sudo et al. (1978), and Al-Duri and McKay (1991) fitted adsorption rates in finite-bath batch systems with the assumption that D_s remains constant throughout the course of adsorption and observed that the resulting D_s values increased with initial solute concentration in the solution. Using the following expression which shows the surface diffusion coefficient to increase exponentially with surface coverage:

$$D_s(q) = D_o \exp\{k(q/q_{sat})\} \tag{2}$$

they were able to successfully correlate the constant D_s values thus obtained to either the surface concentration in equilibrium with the initial solution concentration, q_o or to the surface concentration at equilibrium, q_e. Equation 2 was derived by Neretnieks (1976) by assuming a linear dependence of ΔH_{st} on q in Eq. 1. However, since the solute surface concentration q during such experiments increases from zero to an equilibrium value q_e, according to Eq. 2, the value of D_s does not remain constant during these experiments but, instead, increases continuously with time until equilibrium is attained. Therefore, the correct use of Eq. 2 requires its incorporation in the adsorption model to account for the continuous variation of D_s with q. This was recently done by several investigators (Muraki et al., 1982; Seidel and Carl, 1989; Friedrich et al., 1988) who were then able to successfully fit adsorption rates in finite-bath batch systems for several solute/activated carbon systems.

Previous desorption studies

Desorption of organics from activated carbon in the liquid phase and, especially in aqueous solutions, has received relatively little attention. The majority of available studies have focused on the effectiveness of adsorbate extraction by organic solvents (cf. Cooney et al., 1983; Posey and Kim, 1987; Grant and King, 1990) or supercritical CO_2 (cf. Modell et al., 1980; Tan and Liou, 1989; Srinivasan et al., 1990) for the regeneration of spent activated carbon. The effects of the various relevant parameters on the desorption of a solute from the adsorbent surface (for example, surface loading, sorbent and sorbate characteristics, and so on) have so far not been clarified adequately. Furthermore, modeling of the desorption dynamics has been addressed in only a few studies (Tan and Liou, 1989; Recasens et al., 1989; Srinivasan et al., 1990).

Irreversible solute adsorption on a sorbent surface can be described as the combined result of the formation of permanent bonds between the solute and the surface (chemisorption) and the irreversible transformation of the adsorbed solute into other species through chemical reactions catalyzed by the adsorbent surface. A review of the available studies (cf. Yonge et al., 1985; Rudling and Björkholm, 1987; Grant and King, 1990) indicates that the extent of adsorption irreversibility depends strongly on the particular sorbate/sorbent/solvent system under study. For a particular sorbate/sorbent system, the selection of the solvent used for sorbate extraction has been shown to greatly affect the degree of adsorption irreversibility observed (cf. Cooney et al., 1983; Grant and King, 1990). Water was shown to be a poor extractant of phenolics from

activated carbon. Other determining factors are the chemical properties of the sorbate and the sorbent surface. For a particular adsorbent, irreversible adsorption increases with sorbate molecular reactivity which, in turn, depends on the nature of the sorbate and the solution pH (Yonge et al., 1985; Grant and King, 1990). Adsorption of nonpolar relatively inert compounds was found to be fully or almost fully reversible (Rudling and Björkholm, 1987; Grant and King, 1990). For a particular sorbate, adsorption irreversibility can vary widely for different adsorbents (Goto et al., 1986; Rudling and Björkholm, 1987; Grant and King, 1990). Both oxygenated functional groups and various metals (for example, Mn, Fe, Zn) on the adsorbent surface have been shown to be responsible for irreversible adsorption by promoting chemical reactions between the sorbate and the surface (cf. Grant and King, 1990). Finally, the presence of molecular oxygen dissolved in the solution has also been shown to influence the irreversibility of phenol adsorption on activated carbon by participating in oxidation reactions catalyzed by the surface (cf. Grant and King, 1990).

The effect of repetitive adsorption-regeneration cycles on the adsorptive capacity has been addressed for several solute/activated carbon systems. While for some systems a loss in the adsorptive capacity was observed following only the first cycle with no further loss in subsequent cycles (cf. Modell et al., 1980; Posey and Kim, 1987), for other systems the adsorptive capacity decreased gradually to a constant value over a number of cycles (cf. Modell et al., 1980; Cooney et al., 1983; Goto et al., 1986; Grant and King, 1990).

Experimental

Materials/analytical methods

Toluene adsorption and desorption studies were conducted using Filtrasorb-300 (F-300) activated carbon (Calgon Co., Pittsburgh, PA). Toluene and methanol (HPLC grade) were supplied by Fisher Scientific, Fair Lawn, NJ. All aqueous toluene solutions were prepared in distilled, deionized and activated carbon-treated water from a Milli-Q water treatment system (Millipore Corp., Bedford, MA).

Toluene concentrations in both aqueous solutions and methanol (MeOH) extracts from the regeneration of spent F-300 were measured using a Varian Cary3 UV-Visible spectrophotometer at 206 nm. Because of the possibility that solvent regeneration of spent activated carbon could lead to the desorption of products of catalytic reactions promoted by the activated carbon surface, the adequacy of UV-spectrophotometry for the analysis of the MeOH extracts was first established by chromatographic analysis of several extract samples using a Varian 3700 Gas Chromatograph equipped with a PID detector (EPA Method 8020, direct injection in a glass column packed with 5% SP-1200 and 1.75% Bentone-34 on Supelcoport). The GC analysis showed that toluene was the only detectable aromatic compound in the MeOH samples.

Activated carbon characterization

Surface area, total pore volume and pore-size distribution measurements were conducted by obtaining the adsorption isotherm of N_2 on F-300 activated carbon at 77.5 K using an Autosorb-1 Gas Sorption System (Quantachrome Corp., Syosset, NY). The surface area determination was based on a five-point nitrogen BET at relative N_2 pressures between 0.06 and 0.10. The pore-size distribution computation was based on a slit-shape pore model.

Particle size and shape characteristics for the F-300 activated carbon were studied by image analysis. A frame of several activated carbon particles positioned in random orientation on white background was taken with a Panasonic WV BL600 video camera, digitized and displayed on the screen of a Macintosh IIx personal computer equipped with a frame grabber (Model QuickCapture, Data Translation). Size and shape analysis for the particles on the digitized frame was conducted using the v7.1 Image Analyst software (Automatrix Inc., Billerica, MA). The resolution of the image analysis system used in the present study was found to be about 5%. Based on the information obtained, the diameter of a particle in the sample was determined as the diameter of a circle with an area equal to the projected area of the particle (projected-area diameter).

Adsorption isotherm studies

The equilibrium isotherm for toluene adsorption from an aqueous solution on F-300 activated carbon was determined at 25 ± 1°C using a bottle-point procedure. In order to accelerate the attainment of equilibrium, the experiments were conducted using pulverized activated carbon (U.S. mesh no. 200×325). Prior to its use, the activated carbon was repeatedly rinsed with Milli-Q water to remove the fines, dried overnight at 110°C and stored under vacuum in a desiccator.

Different amounts of activated carbon were weighed and added into each from a batch of six to ten glass bottles (0.26 L). The bottles were then filled with toluene solution which had been prepared in stock overnight, covered with Teflon-lined caps and stirred with magnetic stirrers at the maximum speed. Preliminary transient experiments conducted using the U.S. mesh no. 200×325 sieve fraction indicated that adsorption equilibrium was reached in only a few hours with no appreciable further decrease in the toluene bulk concentration for time periods up to 7 days. Based on these results, the duration of the equilibrium experiments in the isotherm bottles was selected to be 24–36 h. In order to avoid any toluene volatilization during the course of the experiments, no headspace was left in the isotherm bottles. Although preliminary tests indicated no significant toluene losses from the isotherm bottles in the absence of activated carbon, two blanks were included in each batch and were used to determine the initial concentration in the bottles within the batch. In this way, any minimal toluene losses due to adsorption on the glass bottles, the Teflon-coated stirrers and the Teflon-lined caps were accounted for.

Upon equilibration, stirring was stopped and samples from each bottle were taken with a glass syringe, filtered through 0.45-μm Gelman Teflon syringe filters (13 mm in diameter) and analyzed. Separate tests indicated some limited adsorption of toluene on the filter membranes, which resulted in the concentrations of the filtered samples to be about 3–5% lower than the actual values. The measured concentrations were corrected for this error and the mass of toluene adsorbed on the activated carbon was found from a mass balance. The adsorption isotherm data obtained were verified by repeating some of the isotherm experiments using a larger liquid volume (4 L) or a smaller particle size (15–20 μm). All results were within 5% of those obtained previously, indicating that neither

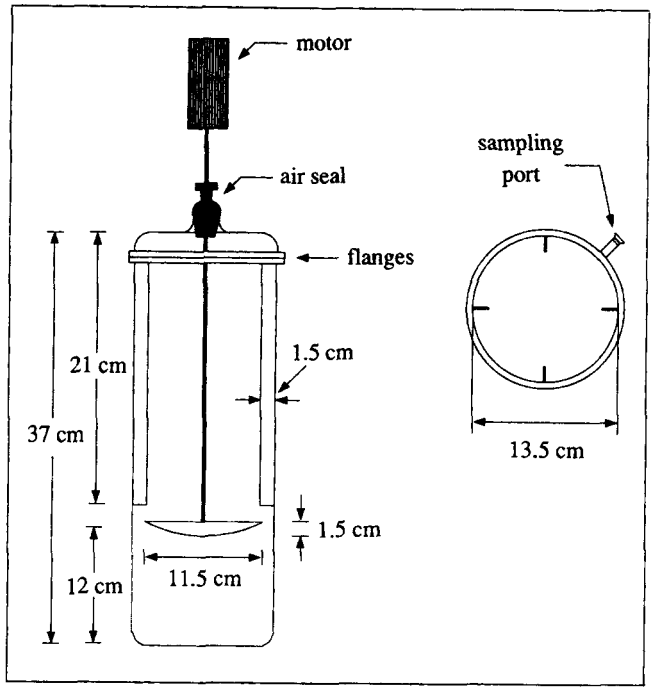

Figure 1. Batch reactor used for the adsorption and desorption rate experiments.

of these factors affected the accuracy of the determined adsorption isotherm.

Adsorption rate studies

Adsorption rate studies were conducted in a batch reactor at 25 ± 1°C by monitoring the decrease in the toluene solution concentration with time. The experiments were conducted using the U.S. mesh no. 14×16, 16×20 and 20×25 sieve fractions which cumulatively constitute the largest fraction of commercial F-300 activated carbon. Prior to their use, all three sieve fractions were treated as described earlier. The reactor consisted of a 4.75-L closed cylindrical Pyrex glass vessel equipped with four stainless steel baffles and a sampling port with a rubber septum which allowed for the withdrawal of samples from the center of the reactor without interrupting the experiments. The solution was stirred with a crescent-shape two-blade borosilicate glass paddle impeller, attached to a borosilicate glass shaft (ACE Scientific Supply Co., East Brunswick, NJ). The impeller was driven by an IKA RW20 motor equipped with a speed controller (Baxter Diagnostics Inc., Scientific Products Division, McGaw Park, IL). In order to minimize the power input required for a fairly homogeneous particle suspension while maintaining well-mixed conditions over the entire liquid volume, the impeller was positioned 12 cm above the vessel bottom. Also, in order to minimize possible toluene volatilization from the vessel, the reactor was kept airtight by use of an air seal equipped with an O-ring (ACE Scientific Supply Co., East Brunswick, NJ) around the stirrer shaft at the point where the shaft entered the vessel. A schematic diagram and the dimensions of the batch reactor are shown in Figure 1.

Toluene solution was prepared in the reactor overnight, leaving no headspace in order to minimize any possible toluene loss due to volatilization. Prior to the initiation of the experiments, the stirring motor was set to a predetermined speed, the solution concentration was measured and a preweighed mass of activated carbon was added to the solution. Liquid samples were withdrawn from the reactor at regular time intervals using glass syringes and were immediately analyzed. The total solution volume reduction due to sampling was less than 2% for all experiments, so that adsorption rates were measured under essentially constant liquid volume.

Desorption isotherm studies

Desorption isotherm experiments were conducted at 25 ± 1°C to determine the degree of toluene adsorption irreversibility on F-300. Different amounts of pulverized activated carbon were loaded in glass bottles (250–550 ml) covered with glass stoppers with predetermined toluene surface concentrations following the procedure described earlier for the adsorption isotherm studies. Upon equilibration, and measurement of the liquid-phase toluene concentration in each bottle, the activated carbon was separated from the solution by vacuum filtration on preweighed glass fiber filters (0.45 μm) and rinsed from the filter back into the empty bottles using Milli-Q water. The bottles were then filled with Milli-Q water leaving no headspace and covered with the glass stopper. The slurry was stirred for four to five days to ensure equilibration and the liquid-phase toluene concentration was measured again. The glass fiber filters used for recovering the loaded activated carbon were dried at 110°C overnight and reweighed to account for any activated carbon that remained attached to them. In all cases, the difference between the filter weights before and after their use was negligible relative to the F-300 amounts used in the experiments.

Desorption rate studies

Aqueous-phase desorption rate experiments were conducted at 25 ± 1°C in the batch reactor described earlier (Figure 1) using the U.S. mesh no. 14×16 and 20×25 sieve fractions. Preweighed F-300 amounts were loaded with different toluene surface concentrations by contacting with an aqueous toluene solution for about 4–6 days at 300 rpm in a 4.8-L glass vessel having a funnel-shaped bottom to facilitate particle recovery after loading. Because concentration measurements during loading indicated very low rates of toluene removal from the solution after the second day, which based on the results from blank runs could be accounted for by minimal toluene volatilization and/or adsorption on the vessel, the toluene surface concentration at loading completion was determined from the adsorption isotherm since 4–6 days should be sufficient for the solution-activated carbon-vessel system to reach equilibrium.

At the end of the loading period, the solution was drained from the loading vessel while the toluene-loaded particles were retained on a fine mesh screen. The particles were then transferred from the screen into the batch reactor, which had previously been filled with Milli-Q water leaving no headspace, the stirrer speed was set to 600 rpm and the solution concentration was monitored with time. On the average, the time elapsed between the recovery of the loaded activated carbon

and the initiation of the desorption experiments was only about 5 min, thus any losses of adsorbed toluene from the particles by volatilization during this short transition period are not likely to be significant. Any minimal particle attrition during the loading period was accounted for by vacuum filtering the solution recovered from the loading vessel on preweighed glass fiber filters (0.45 μm), drying the filters overnight at 110°C and reweighing. In all cases, the attrited F-300 mass was less than 1% of the mass initially added to the loading vessel.

Activated carbon regeneration studies

Preweighed amounts of activated carbon were loaded with a predetermined toluene surface concentration following the procedure described earlier for the desorption rate studies, with the only exception that the loading time was decreased to about 3 days to minimize any toluene losses from the solution not related to adsorption on the activated carbon. Although, at the end of the loading period, the toluene surface concentrations determined from a mass balance and from the adsorption isotherm were in good agreement, the adsorption isotherm value was used for reasons of compatibility. After recovering, the loaded particles were transferred into a 30-mL glass vial where the adsorbed toluene was extracted by methanol following a repetitive batch extraction procedure. The procedure involved adding 25 mL MeOH (about 2.5 mL/g of activated carbon) into the vial and shaking for 1 h with a wrist-action shaker. Shaking was gentle in order to avoid particle attrition during the extraction. At the end of the extracting period the extract was analyzed, drained carefully so that no particles were lost and extraction was resumed by adding a new batch of MeOH. Typically, 95% of the total extractable toluene was recovered in the first three batches. Since extraction rates in subsequent batches were anticipated to be slow because of the low toluene solid-phase concentrations, the extraction time in these batches was increased to about 24 h. Extraction was continued until the toluene extracted in a given batch was insignificant with respect to the toluene mass initially adsorbed on the particles (for example, less than 0.5%). Generally, seven extraction batches were sufficient for the recovery of all extractable toluene. Any minimal activated carbon losses by attrition during particle loading and extraction were carefully accounted for as described earlier.

Model Description

A combined external mass-transfer-homogeneous surface diffusion model (HSDM) was selected for use in this study because of its simplicity, its adequacy in describing adsorption of organics from the aqueous phase on activated carbon (cf. Hand et al., 1983), and also, because of the unimodal pore-size distribution of F-300 activated carbon. The model assumes isotropic adsorbent particles with uniform pores and no preferential pore direction. The solute diffuses through the boundary layer surrounding the adsorbent particles and adsorbs on their external surface. Diffusion inside the particle is assumed to take place only on the pore walls (surface diffusion) with the contribution of pore diffusion being assumed negligible. The effective surface diffusion coefficient D_s can either be constant or dependent on the surface concentration. Equation 2 was used to allow both for a concentration-independent $D_s\,(k=0)$ and a concentration-dependent $D_s\,(k\neq 0)$. Other assumptions involved in the model include spherical adsorbent particles, isothermal conditions and fast intrinsic adsorption kinetics, resulting in equilibrium between the solid-phase and liquid-phase solute concentrations at the external surface of the particles.

The solute diffusion inside a spherical adsorbent particle is described by the following equation:

$$\frac{\partial q}{\partial t}=\frac{D_o}{r^2}\frac{\partial}{\partial r}\left[r^2\exp\{k(q/q_{\text{sat}})\}\frac{\partial q}{\partial r}\right] \tag{3}$$

along with the initial (IC) and boundary conditions (BC):

$$\text{IC:}\quad t=0,\quad 0\le r\le R\quad q=0\qquad \text{(adsorption)} \tag{4a}$$

$$q=q_{o,\text{rev}}\qquad \text{(desorption)} \tag{4b}$$

$$\text{BC:}\quad t>0,\quad \left.\frac{\partial q}{\partial r}\right|_{r=0}=0 \tag{5}$$

$$D_o\rho_s\exp\{k(q/q_{\text{sat}})\}\left.\frac{\partial q}{\partial r}\right|_{r=R}=k_f(C-C_s) \tag{6}$$

Integrating Eq. 3 between $r=0$ and $r=R$ and combining with Eq. 6 yields a new form of the BC at $r=R$:

$$\frac{\partial}{\partial t}\int_0^R qr^2dr=\frac{k_fR^2}{\rho_s}(C-C_s) \tag{7}$$

The solute mass balance in the liquid phase and the relevant ICs are:

$$V_f\frac{dC}{dt}=-\frac{3W}{\rho_sR}k_f(C-C_s) \tag{8}$$

$$\text{IC:}\quad t=0,\quad C=C_o\qquad \text{(adsorption)} \tag{9a}$$

$$C=0\qquad \text{(desorption)} \tag{9b}$$

At the solid-liquid interphase, the solid-phase and the liquid-phase solute concentrations are related through the equilibrium isotherm. For the Fritz-Schlünder isotherm (Table 3):

$$\left.q\right|_{r=R}=\frac{\alpha_1C_s^{\beta_1}}{1+\alpha_2C_s^{\beta_2}} \tag{10}$$

Using the dimensionless quantities:

$$u=\frac{C}{C_o},\quad u_s=\frac{C_s}{C_o},\quad \eta=\frac{q}{q_o},\quad \rho=\frac{r}{R},\quad \tau=\frac{D_ot}{R^2},$$

$$Bi=\frac{k_fRC_o}{\rho_sD_oq_o},\quad A=\frac{3Wq_o}{V_fC_o},\quad K=\frac{1}{\alpha_2C_o^{\beta_2}}, \tag{11}$$

the above set of equations can be rendered dimensionless as follows:

$$\frac{\partial \eta}{\partial \tau} = \frac{1}{\rho^2}\frac{\partial}{\partial \rho}\left[\rho^2 \exp\{k(\eta/\eta_{sat})\}\frac{\partial \eta}{\partial \rho}\right] \quad (12)$$

IC: $\tau = 0, \quad 0 \le \rho \le 1 \quad \eta = 0$ (adsorption) (13a)

$$\eta = \eta_{o,rev} \quad \text{(desorption)} \quad (13b)$$

BC: $\tau > 0, \quad \left.\frac{\partial \eta}{\partial \rho}\right|_{\rho=0} = 0 \quad (14)$

$$\frac{\partial}{\partial \tau}\int_0^1 \eta \rho^2 d\rho = Bi(u - u_s) \quad (15)$$

$$\frac{du}{d\tau} = -ABi(u - u_s) \quad (16)$$

IC: $\tau = 0, \quad u = 1$ (adsorption) (17a)

$$u = 0 \quad \text{(desorption)} \quad (17b)$$

$$\eta\Big|_{\rho=1} = \frac{(K+1)u_s^{\beta_1}}{K + u_s^{\beta_2}} \quad (18)$$

The method of orthogonal collocation (Villadsen and Michelsen, 1978) was used to convert the above set of equations into a set of ODEs which was subsequently solved with an integrator based on Gear's implicit method with adaptive step control. In the case of $k = 0$ in Eq. 12, the resulting set of ODEs is linear and use of five collocation points was sufficient for a converging solution. However, in the case of $k \neq 0$, the resulting set of ODEs is nonlinear and a larger number of collocation points were required to yield a solution independent of the number of collocation points used, the actual number increasing with increasing k and Biot number. Convergence required the use of more than 11 collocation points for the values of k and Bi found by regression of the adsorption rate data in this study and up to 40 collocation points in the limiting case of no external mass-transfer resistance ($Bi \to \infty$).

It is apparent that the assumption of a concentration-dependent D_s ($k \neq 0$) leads to a large increase in the number of collocation points required for model solution. This can be explained considering that, as k increases, the variation in the value of D_s along the radial direction also increases. For large k values, the surface diffusion coefficient D_s is large close to the external particle surface and small close to its center, giving rise to a steep intraparticle surface concentration profile, similar to that predicted by a "shrinking-core" model. In order for a numerical solution to capture the steepness of this profile, the discretization along the radial direction has to provide, at each time step, a sufficiently fine grid at the position of the surface concentration front. Orthogonal collocation is not the best method to solve problems of this type since, for a given choice of Jacobi polynomials, the discretization along the radial direction is determined exclusively by the number of collocation points (Finlayson, 1980). In this case, a moving finite-element scheme with a finely discretized element following the surface concentration front or a finite-difference scheme with a sufficiently fine discretization along the radial direction should be preferable. However, this was not attempted and the orthogonal collocation scheme was retained because of its simplicity.

Table 1. Physical Properties of F-300 Activated Carbon

Surface area* (m^2/g):	
U.S. mesh no. 200×325	1,030
U.S. mesh no. 20×25	970
Skeletal density** (g/cm^3)	2.13
Pore volume† (cm^3/g):	
Micropores ($d_p < 20$ Å)	0.425
Mesopores ($20 < d_p < 500$ Å)	0.160
Macropores ($d_p > 500$ Å)	0.305
Total	0.890
Apparent density‡ (g/cm^3)	0.735
Particle porosity‡	0.654

*Five-point N_2 BET at relative pressures between 0.06 and 0.1.
**Measured by He pycnometry.
†Combined N_2 condensation ($d_p < 1{,}200$ Å) and Hg porosimetry ($d_p > 1{,}200$ Å) measurement.
‡Calculated from the experimentally measured quantities.

Results and Discussion

Adsorbent characterization

The physical properties of F-300 are given in Table 1. The pore-size distribution is unimodal with a peak in the micropore region ($d_p < 20$ Å). It is noteworthy that the surface area of pulverized F-300 (US mesh no. 200×325) was found to be somewhat larger than that of much larger particles (US mesh no. 20×25). Mattson and Mark (1971) reported that for some activated carbons the nitrogen BET surface area increases significantly with decreasing particle size. They argued that particle grinding might lead to the opening of pores which were previously inaccessible, thus, increasing the surface area available for adsorption of nitrogen. However, this increase in the BET surface area may not necessarily lead to a higher capacity for adsorption of organics from an aqueous solution due to size exclusion effects. Peel and Benedek (1980), among others, have shown that, given sufficient time for the attainment of equilibrium, the adsorption capacity of large activated carbon particles is similar to that of pulverized activated carbon. This was also confirmed in this study.

The use of image analysis provides particle-size distributions by number. Figure 2 shows the cumulative undersize particle-size distributions for three F-300 sieve fractions used in the rate experiments, based on a sample size of 130 particles for each sieve fraction. All three particle-size distributions approximately follow the log-normal distribution, as indicated by the nearly straight distribution lines on a log-normal plot. The small deviations from linearity observed at both ends for all three distributions result from the relatively small size of the samples analyzed and from the fact that the particle diameters within a particular sieve fraction do not range from zero to infinity, as the log-normal distribution requires, but they rather lie between two finite values dictated by the openings in the upper and lower sieves.

Particle size and shape characteristics for the same three F-300 sieve fractions are summarized in Table 2. The Sauter mean of a particle-size distribution represents an effective surface-to-volume particle diameter and is the most appropriate mean particle diameter to use in applications, like adsorption

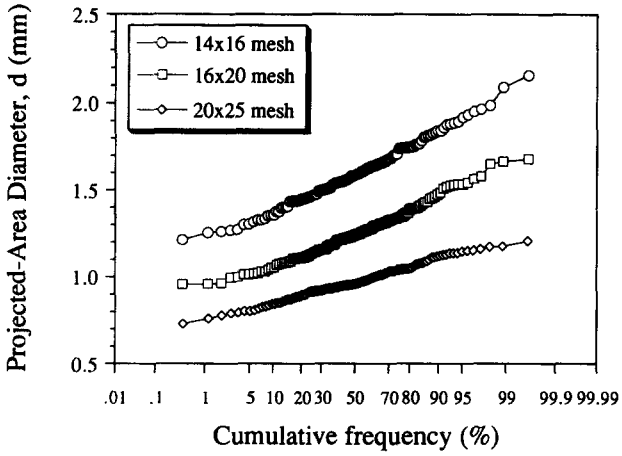

Figure 2. Cumulative undersize particle-size distributions by number for F-300 activated carbon.

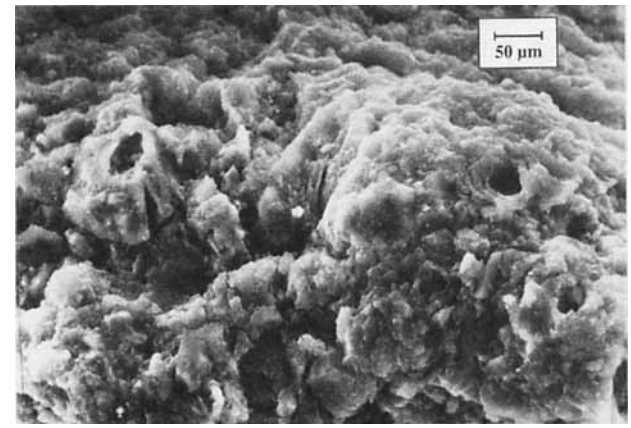

Figure 3. Scanning electron micrograph of the external surface of F-300 activated carbon.

on activated carbon, where external mass-transfer resistance is significant (cf. Mathews and Zayas, 1989). It is noteworthy that the arithmetic and the geometric means of the sieve openings are significantly lower than both the length mean and the Sauter mean particle diameters for all three sieve fractions. This is because, as can be seen in Figure 2, the projected-area diameter of most particles in a particular sieve fraction is larger than the size of the openings in the upper sieve. Similar results have been reported for other activated carbons (Mathews, 1983; Mathews and Zayas, 1989). Mathews and Zayas (1989) also reported that a given sieve fraction of GAC 40 activated carbon contains particles with a projected-area diameter smaller than the openings in the lower sieve. This could possibly result from incomplete sieving and was not observed in the present study. Based on the above results, use of either the arithmetic or the geometric mean of the sieve openings as a measure of the effective particle size in fitting activated carbon adsorption rate data should be avoided as this would lead to an underestimation of the effective diffusion coefficient.

The roundness of a particle's projected area can be used as a measure of particle sphericity. Its maximum possible value of 1 is attained when the projected area is perfectly circular. Another measure of particle sphericity is the aspect ratio (major to minor axis length ratio) of the particle's projected area when the latter is approximated by an ellipse. An aspect ratio close to 1 indicates a nearly spherical particle whereas a larger value indicates an elongated particle. Table 2 shows that, on the average, the F-300 particles are somewhat elongated and, also, that their shape does not change significantly with size. The relatively elongated shape of the particles allows them to pass through the openings of a sieve with their long axis normal to the sieve plane, thus, explaining how the majority of the particles within a given sieve fraction could have a larger projected-area diameter than the openings in the upper sieve (Figure 2).

The morphology of the external surface of F-300 activated carbon was studied by Scanning Electron Microscopy (SEM). A typical micrograph is shown in Figure 3. It is apparent that the external surface of F-300 is quite rough, consisting of cavities, cracks, and irregular protrusions. High surface roughness tends to impede mixing close to the particle surface, leading to a thick boundary layer around the particles and an increase in the external mass-transfer resistance.

Adsorption isotherm studies

The adsorption equilibrium data were fitted with several well-known isotherm models using the Marquardt-Levenberg optimization procedure to minimize the root mean square of

Table 2. Particle Size and Shape Characteristics of F-300 Activated Carbon

U.S. Mesh No. Sieve Fraction	Arithmetic Mean of Sieve Openings (mm)	Geometric Mean of Sieve Openings (mm)	Sauter Mean Diameter* d_{sv} (mm)	Length Mean Diameter** d_{ave} (mm)	Average Aspect Ratio (Major/Minor Axis)	Average Roundness†
14×16 (0.71–0.85 mm)	1.295	1.298	1.643	1.600	1.53	0.84
16×20 (0.85–1.18 mm)	1.015	1.001	1.295	1.255	1.38	0.87
20×25 (1.18–1.41 mm)	0.780	0.777	0.998	0.974	1.47	0.85

$^{*}d_{sv}=\dfrac{\sum_{i=1}^{N_p} d_i^3}{\sum_{i=1}^{N_p} d_i^2}$, $^{**}d_{ave}=\dfrac{\sum_{i=1}^{N_p} d_i}{N_p}$, $^{\dagger}\text{Roundness}=\dfrac{4\pi\cdot\text{Area}}{(\text{Perimeter})^2}$

Table 3. Parameter Values from Fitting the Adsorption Equilibrium Data with Various Isotherms Models

Isotherm Model		Concentration Range (mg/L)	Parameter Values*	Normalized RMS (%)**	Nonnormalized RMS†
1) Langmuir:	$q_e = \frac{K_L \cdot q^o \cdot C_e}{1 + K_L \cdot C_e}$	$0.7 < C_e < 50$	$K_L = 0.499$, $q^o = 250.3$	7.34	—
2) Freundlich:	$q_e = K_F \cdot C_e^{n_F}$	$0.7 < C_e < 50$	$K_F = 99.5$, $n_F = 0.278$	6.74	—
		$C_e < 1.35$	$K_F = 90.5$, $n_F = 0.517$	2.87	—
		$1.35 < C_e < 25$	$K_F = 104.0$, $n_F = 0.277$	2.01	—
		$C_e > 25$	$K_F = 220.2$, $n_F = 0.0426$	0.89	—
3) Radke-Prausnitz:	$q_e = \frac{a_1 \cdot a_2 \cdot C_e}{1 + a_2 \cdot C_e^b}$	$0.7 < C_e < 50$	$a_1 = 150.8$, $a_2 = 1.544$, $b = 0.842$	3.05	5.531
4) Toth:	$q_e = \frac{K_T \cdot q_T \cdot C_e}{[1 + (K_T \cdot C_e)^{n_T}]^{1/n_T}}$	$0.7 < C_e < 50$	$q_T = 380.5$, $K_T = 1.519$, $n_T = 0.422$	2.9	4.738
5) Fritz-Schlünder:	$q_e = \frac{\alpha_1 \cdot C_e^{\beta_1}}{1 + \alpha_2 \cdot C_e^{\beta_2}}$	$0.7 < C_e < 50$	$\alpha_1 = 120.03$, $\alpha_2 = 0.3060$, $\beta_1 = 0.5675$, $\beta_2 = 0.5955$	2.91	4.488

*Units: K_L [=] L/mg, q^o [=] mg/g, K_F [=] (mg/g) (L/mg)^{n_F}, n_F [=] dimensionless, α_1 [=] (mg/g) (mg/L)$^{b-1}$, α_2 [=] (mg/L)$^{-b}$, b [=] dimensionless, K_T [=] L/mg, q_T [=] mg/g, n_T [=] dimensionless, α_1 [=] (mg/g) (mg/L)$^{-\beta_1}$, α_2 [=] (mg/L)$^{-\beta_2}$, β_1, β_2 [=] dimensionless.

**Normalized RMS $= 100 \times \sqrt{\frac{1}{N_{pt}} \cdot \sum_{i=1}^{N_{pt}} \left(\frac{q_{ei,exp} - q_{ei,calc}}{q_{ei,exp}} \right)^2}$

†Nonnormalized RMS $= \sqrt{\frac{1}{N_{pt}} \cdot \sum_{i=1}^{N_{pt}} (q_{ei,exp} - q_{ei,calc})^2}$

the normalized residuals (normalized RMS). The results of the fitting procedure are presented in Table 3. For those cases where two models yielded approximately the same normalized RMS value, the RMS of the nonnormalized residuals (nonnormalized RMS) was computed and used as a second criterion for determining the effectiveness of a particular model to fit the adsorption isotherm data. It should be noted that, because it weighs the actual error at all points, the nonnormalized RMS is more sensitive to errors at high equilibrium solution concentrations. This, however, is not true for the normalized RMS, which is based on the relative error and, therefore, weighs all points equally.

The Langmuir isotherm gave the poorest fit, deviating considerably at high liquid concentrations and slightly less at low concentrations. The Freundlich isotherm yielded an excellent overall fit, but required a different representation of the isotherm in each of the three distinct liquid concentration ranges shown in Table 3. Use of only one representation over the entire liquid concentration range resulted in a significantly worse correlation. The need for a piecewise Freundlich fit of the adsorption isotherm has also previously been reported for other sorbate/activated carbon systems (cf. Fritz and Schlünder, 1981; Noll et al., 1992). Between the two three-parameter models investigated in this study, the rarely used Toth isotherm (Toth, 1971) gave a somewhat better fit than the better known Radke-Prausnitz isotherm (Radke and Prausnitz, 1972). Although both models provided a satisfactory fit to the isotherm data over most of the liquid concentration range, neither of them described accurately the flat portion of the experimental isotherm curve. In order to overcome this problem, the empirical four-parameter Fritz-Schlünder isotherm (Fritz and Schlünder, 1974) was tried with the expectation that the introduction of a fourth parameter would enhance the fit to the flat portion of the isotherm. Although use of this isotherm did not improve the overall fit, yielding a normalized RMS value close to those obtained with the three-parameter isotherms, it did improve somewhat the fit at high concentrations and was, therefore, selected for further use. Figure 4 compares the experimentally determined adsorption isotherm data to the fit following the Fritz-Schlünder isotherm.

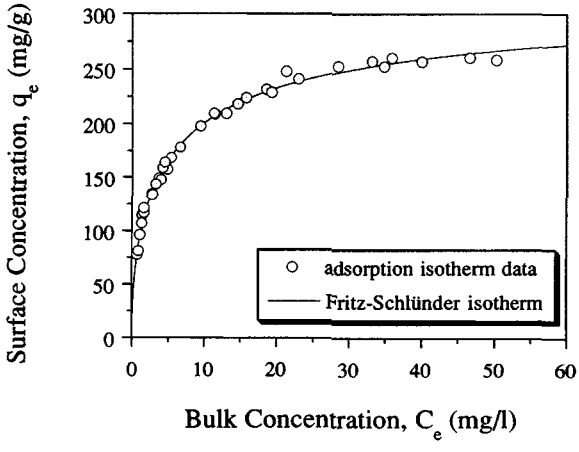

Figure 4. Equilibrium isotherm for toluene adsorption on F-300 activated carbon at 25°C.

Adsorption rate studies

The effects of the initial solution concentration, the particle size and the hydrodynamic conditions in the liquid phase on the rate of toluene adsorption on F-300 activated carbon were investigated in a series of finite-bath batch adsorption rate experiments. Experiments were carried out for three initial

Table 4. Results from Nonlinear Regression of the Adsorption Rate Experiments Assuming D_s is Constant

Run No.	d_p (mm)	C_o (mg/L)	W (g)	N (rpm)	$D_s \times 10^8$ (cm^2/s)	$k_f \times 10^3$ (cm/s)	RMS of Normalized Residuals (%)
1	0.998	11.0	0.554	600	1.07	10.85	1.02
2	0.998	38.2	0.775	600	4.55	10.03	0.89
3	0.998	59.5	0.975	300	7.51	7.24	1.44
4	0.998	60.9	0.975	450	7.39	8.59	0.91
5	0.998	63.0	0.975	600	7.18	10.51	1.04
6	0.998	61.2	0.975	800	7.46	12.07	1.37
7	1.643	11.7	0.554	600	1.16	9.93	0.80
8	1.643	39.3	0.775	600	3.79	10.43	0.89
9	1.643	60.5	0.975	350	4.35	7.24	0.65
10	1.643	62.3	0.975	600	5.28	11.44	1.38
11	1.643	62.0	0.975	900	5.57	11.17	1.36

toluene concentrations C_o, two particle diameters d_p and several stirring speeds N.

Constant Surface Diffusion Coefficient. Initially, the concentration-dependence of the toluene surface diffusion coefficient D_s was ignored (that is, $D_s = D_o$, $k = 0$ in Eq. 12) and the model was fitted to each experimental adsorption rate curve *separately* to determine the values of the transport parameters, that is, D_s and k_f, that best described the specific data. Fitting was carried out by nonlinear regression using the Marquardt-Levenberg optimization procedure to minimize the RMS of the normalized residuals between the experimental and the computed liquid concentrations. The regression results are presented in Table 4. It is apparent that, for both particle sizes, the assumption of a concentration-independent surface diffusion coefficient results in D_s values which increase as the initial toluene concentration C_o in the solution increases. This is in agreement with results by others (Neretnieks, 1976; Sudo et al., 1978; Fritz et al., 1981; Itaya et al., 1987; Al-Duri and McKay, 1991) and indicates that D_s is indeed concentration-dependent. The predicted constant D_s values also appear to depend on the particle size, with the values for the smaller particles being, in general, larger than those for the larger particles. The predicted values of the external mass-transfer coefficient k_f increase significantly with increasing stirring speed N, as expected, but they appear to be independent of the particle size.

Concentration-Dependent Surface Diffusion Coefficient. Based on the above results a concentration-dependent surface diffusion coefficient $D_s(q)$ was employed to describe the adsorption rate experiments ($k \neq 0$ in Eq. 12). Because of the addition of an extra adjustable parameter (k) and, also, in order to broaden the variation in surface concentration q among the experimental points to be fitted, the results from all experimental adsorption rate curves were pooled and fitted simultaneously. In addition, in order to minimize the total number of parameters to be determined by regression, a solid-liquid mass-transfer correlation was employed to relate the value of the external mass-transfer coefficient k_f to the operating conditions (N, d_p) in the various experiments. Although solid-liquid mass transfer in agitated vessels has attracted significant attention through the years (cf. Brian et al., 1969; Levins and Glastonbury, 1972a; Nienow, 1985), none of the proposed correlations is able to predict k_f reliably under a wide range of hydrodynamic conditions and vessel configurations or to fully describe the effect of all relevant parameters (cf. Boon-Long et al., 1978; Mathews and Zayas, 1989). In this study, the following general expression (cf. Levins and Glastonbury, 1972b; Sano et al., 1974) was used for reasons of simplicity:

$$Sh = \frac{k_f d_p}{D_1} = 2 + B\left(\frac{\bar{\epsilon} d_p^4}{\nu^3}\right)^{\lambda} Sc^{1/3} \tag{19}$$

where B and λ are experimentally determined constants. In most cases, and certainly for the operating conditions employed in this study, the first term on the right side of Eq. 19 can be ignored. Furthermore, it is well established that for turbulent mixing conditions in the vessel, the average power input per unit fluid mass $\bar{\epsilon}$ can be related to the stirring speed N as follows (cf. Tatterson, 1991):

$$\bar{\epsilon} = \frac{N_{po} N^3 D_\alpha^5}{V_f} \tag{20}$$

where N_{po} is the power number characteristic of the vessel geometry. Ignoring the first term in Eq. 19 and combining with Eq. 20, the value of the external mass-transfer coefficient k_f at any operating conditions (N, d_p) can be related to a reference value $k_{f,\text{ref}}$ at some reference set of operating conditions (N_{ref}, $d_{p,\text{ref}}$) as follows:

$$k_f = k_{f,\text{ref}}\left(\frac{d_p}{d_{p,\text{ref}}}\right)^{(4\lambda-1)}\left(\frac{N}{N_{\text{ref}}}\right)^{3\lambda} \tag{21}$$

Equation 21 was incorporated in the adsorption model and all adsorption rate experiments were fitted simultaneously to obtain the combination of D_o, k, $k_{f,\text{ref}}$ ($N_{\text{ref}} = 600$ rpm, $d_{p,\text{ref}} = 1.643$ mm) and λ that best described the set of experiments. The objective function to be minimized was defined as the RMS of the sum of the normalized residuals for all experimental curves:

$$\text{RMS} = 100 \times \sqrt{\frac{\sum_{i=1}^{N_{cu}} \sum_{j=1}^{N_{pt,i}} \left(\frac{u_{j,\text{exp}} - u_{j,\text{calc}}}{u_{j,\text{exp}}}\right)^2}{\sum_{i=1}^{N_{cu}} N_{pt,i}}} \tag{22}$$

The parameter values that best described the combined experimental data were $D_o = 3.59 \times 10^{-9}$ cm^2/s; $k = 5.086$, $k_{f,\text{ref}} = 9.93 \times 10^{-3}$ cm/s ($N_{\text{ref}} = 600$ rpm, $d_{p,\text{ref}} = 1.643$ mm) and $\lambda = 0.179$ with a resulting RMS = 2.34%. The experimentally determined adsorption rate curves for three different initial solution concentrations C_o, a fixed stirring speed ($N = 600$ rpm) and two particles sizes are compared to the model fit in Figure 5. The effect of stirring speed N on the adsorption rate is shown together with the model prediction for the limiting case of no external mass-transfer resistance ($Bi \to \infty$) in Figure 6. It is apparent from Figures 5 and 6 that, with the use of the *same* set of parameters, the model was able to describe successfully the adsorption rate under a wide range of experimental conditions (C_o, d_p, N). Because of the rough external

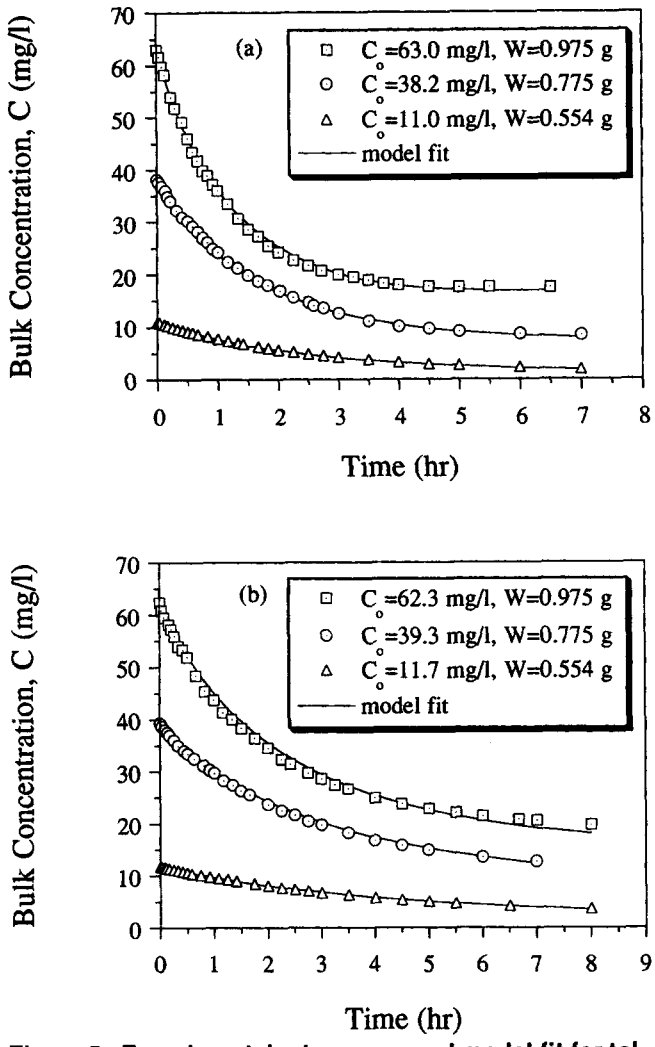

Figure 5. Experimental rate curves and model fit for toluene adsorption on F-300 activated carbon in a batch reactor, $N = 600$ rpm; (a) $d_p = 0.998$ mm; (b) $d_p = 1.643$ mm.

surface of F-300 (Figure 3), external mass-transfer resistance remains significant even under vigorous stirring of the solution (Figure 6). Consequently, caution should be exercised in neglecting external mass-transfer resistance when modeling adsorption on activated carbon from aqueous solutions, as has also been noted by other investigators (Brauch and Schlünder, 1974; Neretnieks, 1976).

Based on the best fit parameter values, the value of the surface diffusion coefficient D_s at surface saturation ($q = q_{sat}$) is almost 160 times larger than its value at $q = 0$, indicating a strong dependence of D_s on surface coverage. Such strong $D_s(q)$ dependencies have also been reported previously by Neretnieks (1976) and Seidel and Carl (1989) for other solute/activated carbon systems. The value of the exponent λ determined in the present study is close to the value 1/6 obtained from the widely accepted equation of Ranz and Marshall (1952) by using Kolmogorroff's theory to express the Reynolds number in a solid suspension (cf. Levins and Glastonbury, 1972b; Nienow, 1985). It is also in good agreement with other values reported in the literature (Levins and Glastonbury, 1972a; Sano et al., 1974). Based on the λ value found in this study, the external mass-transfer coefficient k_f is proportional to $d_p^{-0.284}$ and $N^{0.537}$. Both of these results are in general agreement with other experimental results reported in the literature (cf. Levins and Glastonbury, 1972a; Boon-Long et al., 1978).

In order to verify the ability of the model to describe the rate of adsorption under other operating conditions, an additional rate experiment was conducted using an initial solution concentration, an activated carbon mass and a particle size different from those previously employed in the fitted experiments. The experimental adsorption rate curve is shown together with the model *prediction* in Figure 7. It is evident that the model prediction is excellent, confirming the ability of the external film-HSDM model to successfully describe, with the set of parameters previously obtained, the dynamics of toluene adsorption on F-300 in the batch reactor, at least within the range of operating conditions (C_o, d_p, N) investigated in this study.

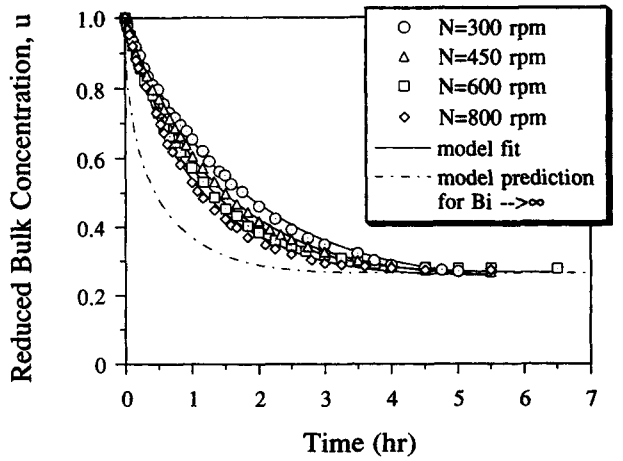

Figure 6. Effect of stirring speed N on the rate of toluene adsorption on F-300 activated carbon in a batch reactor ($C_o \approx 61$ mg/L, $d_p = 0.998$ mm, $W = 0.975$ g).

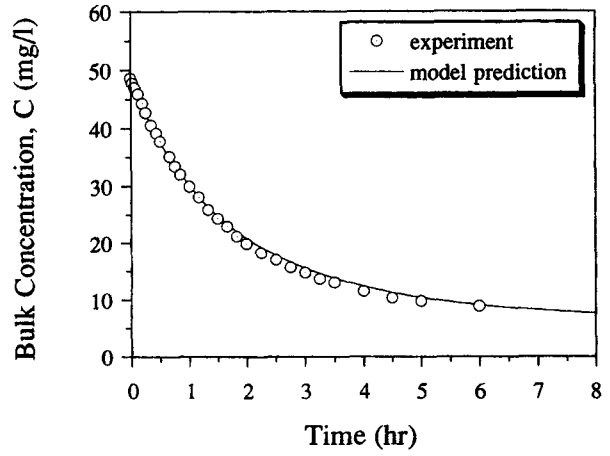

Figure 7. Experimental rate curve and model prediction for toluene adsorption on F-300 activated carbon ($C_o = 48.7$ mg/L, $d_p = 1.295$ mm, $W = 1.093$ g, $N = 600$ rpm).

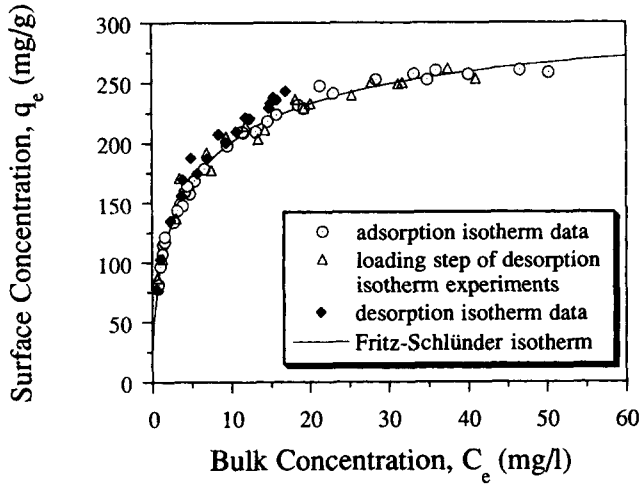

Figure 8. Comparison of the adsorption and desorption equilibrium isotherms for the toluene/F-300 activated carbon system at 25°C.

It is worth noting that, although the use of a surface diffusion coefficient increasing exponentially with surface concentration (Eq. 2) in the HSDM allowed for the successful description of the rate of adsorption, this is not a proof that the dependence of D_s on q is indeed exponential. The use of a D_s which increases linearly with q, according to the form $D_s = D_o\ (1 + k'q/q_{sat})$, also resulted in a good fit of the experimental adsorption rates yielding different D_s values, approximately the same $k_{r,ref}$ ($N_{ref} = 600$ rpm, $d_{p,ref} = 1.643$ mm) and λ values and only a slightly worse overall fit. This suggests that it is the use of a concentration-dependent D_s in the HSDM that is mainly responsible for the successful description of the adsorption rate under a variety of operating conditions with the use of the *same* set of parameters, and not the particular $D_s(q)$ dependence assumed. This is also supported by the fact that adsorption rate data from finite-bath batch experiments have been successfully described in the past incorporating a variety of $D_s(q)$ models in the HSDM (Muraki et al., 1982; Seidel and Carl, 1989; Hutchinson and Robinson, 1990).

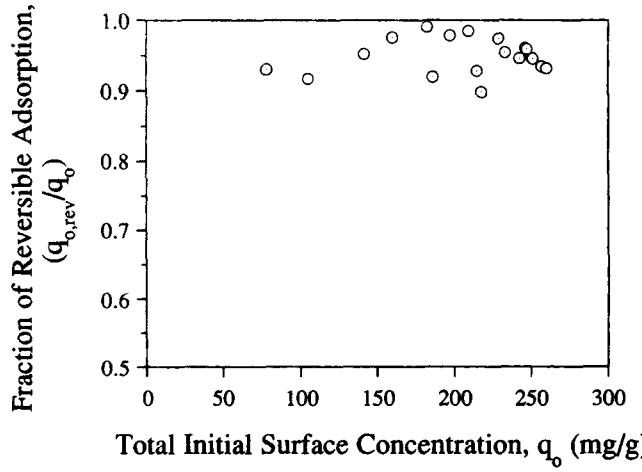

Figure 9. Fraction of reversible toluene adsorption on F-300 activated carbon as a function of the total initial surface concentration.

Desorption isotherm studies

Toluene initial surface concentrations q_o calculated from a mass balance over the loading step were typically within 3% of those predicted by the adsorption isotherm, and the latter values were selected for use in the analysis of the desorption equilibrium experiments. Toluene surface concentrations q_e at desorption equilibrium were found from a mass balance. The results from the adsorption and the desorption isotherm studies are compared in Figure 8. The two sets of data are in good agreement with the desorption isotherm points lying, in general, slightly above the adsorption isotherm ones. Since in the case of a fully reversible adsorption, the two data sets should be statistically indistinguishable, the observed hysteresis between adsorption and desorption in Figure 8 suggests that a small fraction of the toluene was irreversibly adsorbed. It has been suggested that strong adsorption of aromatics on activated carbon can take place through the formation of electron donor-acceptor bonds between the aromatic ring and the surface carbonyl groups (Mattson et al., 1969). The activation energy for toluene desorption from such sites may be so high that, if desorption can indeed occur, its rate is so low that, for all practical purposes, the adsorption of toluene on these sites could be considered essentially irreversible for the given temperature and water as a regeneration solvent.

The initial surface concentration of the reversibly adsorbed toluene $q_{o,rev}$ as well as the fraction of reversible toluene adsorption ($= q_{o,rev}/q_o$) can be computed for each desorption equilibrium experiment as follows: Prior to desorption, the total adsorbed solute can be distinguished into reversibly and irreversibly adsorbed, so that $q_o = q_{o,rev} + q_{o,irrev}$. During the course of desorption, the molecules adsorbed irreversibly will remain bound to the surface while some of those reversibly adsorbed will desorb until equilibrium is established between the solute concentration C_e in the solution and the remaining surface concentration of the reversibly adsorbed solute $q_{e,rev}$. Therefore, at desorption equilibrium, C_e and $q_{e,rev}$ can be related through the adsorption isotherm allowing for the computation of $q_{o,rev}$ from a mass balance:

$$q_{e,rev} = \frac{\alpha_1 C_e^{\beta_1}}{1 + \alpha_2 C_e^{\beta_2}} \tag{23}$$

$$q_{o,rev} = q_{e,rev} + \frac{V_f C_e}{W} \tag{24}$$

The reversible fraction of adsorption ($= q_{o,rev}/q_o$) computed in this manner for 19 desorption isotherm experiments is shown in Figure 9. Since irreversible adsorption is likely to occur on sites with the highest energy of adsorption, which would be occupied irrespective of the surface concentration, the fraction of irreversible adsorption may be expected to be higher at low initial surface concentrations. This, however, was not observed in the present work, possibly because the extent of irreversible adsorption is indeed small (about 5%), and the expected effect may have been "masked" by small experimental errors. The average value of the reversible fractions of adsorption in Figure 9 is about 0.95, with a standard deviation about 0.025.

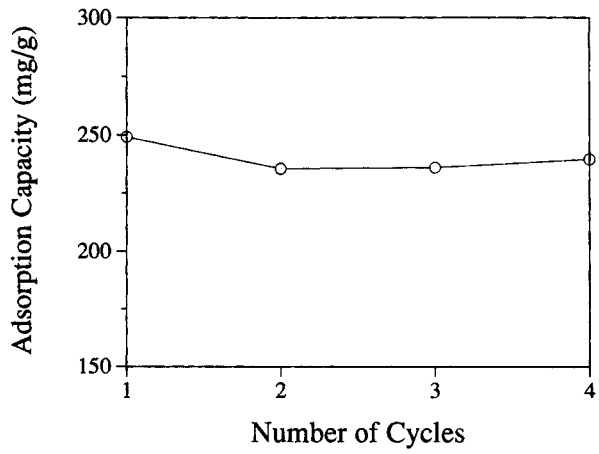

Figure 10. Effect of the number of adsorption/regeneration cycles on the adsorption capacity of F-300 activated carbon for toluene.

Activated carbon regeneration studies

To further study the extent of adsorption irreversibility, toluene-loaded activated carbon was regenerated by methanol extraction, and the toluene mass extracted was compared to the mass initially adsorbed on the surface. Methanol was selected as the extracting solvent because it is a strong toluene solvent, it has a low adsorbability on activated carbon, and it can be easily displaced from activated carbon by water leaching (Cooney et al., 1983). The observed extraction efficiency was about 98% irrespective of initial surface loading. This extraction efficiency is slightly higher than the average fraction of reversible adsorption determined from the desorption isotherm experiments in the aqueous phase (about 95%). Considering that MeOH is a stronger toluene solvent than water, the toluene-surface interactions may be expected to be weaker in MeOH than in water, resulting in a smaller activation energy for desorption from a given site. This would lead not only to higher rates of desorption, but also to a smaller fraction of irreversible adsorption.

In order to investigate the effect of repetitive adsorption-desorption cycles on the adsorption reversibility and the capacity of F-300 for toluene, a batch of activated carbon was exposed to repetitive adsorption-MeOH regeneration cycles. At the end of every extraction, the particles were washed repeatedly with large quantities of Milli-Q water (about 10 L/g of F-300) in a vacuum filtration unit to drive off any MeOH retained in the pores, allowed to dry under vacuum at room temperature for about 24 h, weighed and reloaded with toluene. Conditions during successive loadings (initial toluene concentration, loading time, stirring speed, and so on) were approximately the same so that the adsorption capacities computed from a mass balance for all cycles could be directly compared to each other. The results from these experiments are shown in Figure 10. The capacity of the virgin activated carbon during the first cycle as computed from a mass balance was in excellent agreement with that predicted by the adsorption isotherm. The efficiency of the first extraction was only 93%, resulting in a decrease of about 6% in the computed adsorption capacity between the first and the second cycles. This is in very good agreement with the average fraction of irreversible adsorption (about 5%) determined from the desorption isotherm studies. Adsorption capacities measured in subsequent cycles remained unchanged within experimental accuracy. The above results indicate that all sites that could adsorb toluene irreversibly were essentially exhausted during the first cycle, leading to a fully reversible adsorption in subsequent cycles.

In addition to the above multiple-cycle adsorption-regeneration experiment, two other F-300 samples were exposed to two successive cycles of toluene adsorption followed by MeOH extraction. This time, however, instead of rinsing the particles with water at the end of the first cycle to drive the MeOH out of the pores, the activated carbon was dried at 110°C overnight. For both samples, adsorption capacities as well as extraction efficiencies in the second cycle were in excellent agreement with those observed in the first cycle, indicating that heating the activated carbon at an elevated temperature returned it to its virgin condition. Since higher temperatures result in higher intrinsic rates of desorption, these results suggest that the small fraction of irreversible adsorption observed in water and MeOH was not due to the formation of permanent toluene-surface bonds, but due to the very low rate of toluene desorption from high-energy sites.

Desorption rate studies

Finite-bath batch desorption experiments in the aqueous phase were conducted in order to investigate the effects of the initial toluene surface concentration q_o, the particle diameter d_p and the solid/liquid ratio (W/V_f) on the desorption rates and to examine the ability of the model to predict these rates. The transport parameters D_o, k, $k_{f,\text{ref}}$ and λ used in the model for the computation of the desorption rate curves were those determined earlier by fitting the adsorption rate experiments. External mass-transfer coefficients k_f were calculated using Eq. 21. The total initial toluene concentration q_o value was determined from the adsorption isotherm and the initial surface concentration of the reversibly adsorbed toluene $q_{o,\text{rev}}$ was assumed to be 95% of q_o based on the results from the desorption isotherm studies.

The results from the desorption rate experiments are compared to the model *prediction* in Figure 11. It is apparent that, under all experimental conditions investigated, the model was able to successfully predict both the observed rate of desorption and the toluene solution concentration close to equilibrium. The correct prediction of the approached equilibrium provides an independent confirmation that only 95% of the total initial toluene surface concentration q_o was reversibly adsorbed and was, therefore, available for desorption. Once again, this fraction seems to be independent of the initial surface concentration q_o (Figure 11a). The success of the HSDM in predicting correctly *both* the desorption rate and the approached equilibrium *simultaneously* indicates that the assumption of fast intrinsic desorption kinetics for the *reversibly* adsorbed toluene is indeed valid. If the intrinsic desorption kinetics were rate-limiting, the model should overestimate the rate of desorption even in those cases where it predicted the desorption equilibrium correctly.

Conclusions

The rate of toluene adsorption from an aqueous solution

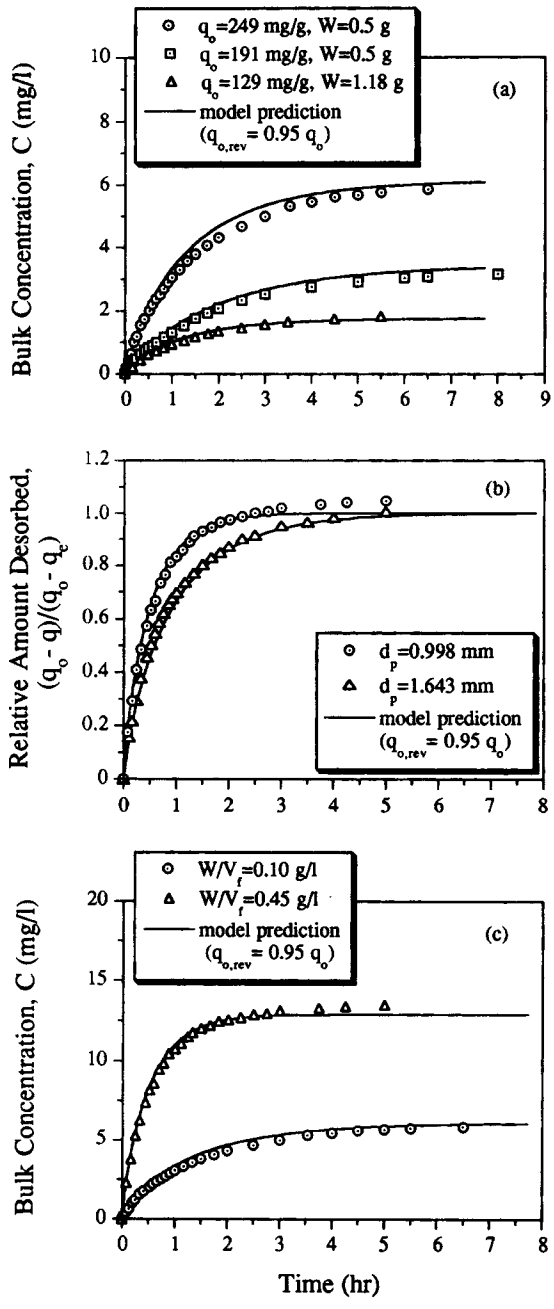

Figure 11. Experimental rate curves and model predictions for toluene desorption from F-300 activated carbon in a batch reactor, N = 600 rpm: (a) effect of q_o, d_p = 0.998 mm; (b) effect of d_p, $q_o \approx$ 255 mg/g, W = 0.5 g; (c) effect of W/V_f ratio, $q_o \approx$ 255 mg/g, d_p = 0.998 mm).

on F-300 activated carbon was measured in finite-bath batch experiments for different toluene initial concentrations, particle sizes and hydrodynamic conditions in the liquid phase. The results were successfully fitted by the HSDM with external mass-transfer resistance and a surface diffusion coefficient which increases exponentially with surface coverage. Use of the transport parameters determined by the fitting procedure allowed for the accurate *prediction* of the adsorption rate under operating conditions different from those employed in the adsorption rate experiments used for fitting. Because of the rough external surface of F-300, external mass-transfer resistance appears to be significant even under vigorous mixing of the liquid phase and should not be ignored in modeling adsorption of organics from an aqueous solution.

The adsorption of toluene on F-300 activated carbon is almost completely reversible. Desorption equilibrium and rate studies in aqueous solutions indicated an average toluene adsorption reversibility in water at 25°C of about 95%. These results appear to be independent of the initial toluene surface concentration on the activated carbon. The rate of toluene desorption from F-300 in a batch reactor was successfully *predicted* by the external film-HSDM for different initial surface concentrations, particle sizes and solid/liquid ratios using the transport parameters determined earlier by fitting adsorption rate experiments in the same reactor.

Methanol extraction was shown to be effective in regenerating toluene-loaded activated carbon resulting in a smaller adsorption irreversibility than that observed in aqueous solutions. Irreversible toluene adsorption was observed only on virgin F-300 activated carbon. Repetitive cycles of adsorption followed by methanol regeneration showed a decrease in the adsorptive capacity after the first cycle but no further decrease in subsequent cycles.

Notation

A = dimensionless quantity defined in Eq. 11 ($=3Wq_o/V_fC_o$)
B = constant defined in Eq. 19
Bi = Biot number ($=k_fRC_o/\rho_sD_oq_o$)
C = solute liquid-phase concentration, mg/L
C_o = initial solute liquid-phase concentration (adsorption) or solute liquid-phase concentration in equilibrium with q_o (desorption), mg/L
d = projected-area particle diameter, mm
d_p = particle diameter, mm
D_α = impeller diameter, mm
D_l = solute diffusion coefficient in the liquid phase, m^2/s
D_o = surface diffusion coefficient at $q=0$, m^2/s
D_s = surface diffusion coefficient, m^2/s
D_{so} = parameter defined in Eq. 1, m^2/s
k = parameter defined in Eq. 2
k_f = external mass-transfer coefficient, m/s
K = dimensionless quantity defined in Eq. 11 ($=1/\alpha_2C_o^{\beta_2}$)
N = impeller speed, rpm
N_{cu} = number of experimental rate curves fitted simultaneously
N_p = particle sample size
N_{po} = power number for the vessel (Eq. 20), L/mm^3
N_{pt} = number of points on a fitted experimental curve
q = solute surface (solid-phase) concentration, mg/g
q_o = solute surface concentration in equilibrium with C_o (adsorption) or initial solute surface concentration (desorption), mg/g
r = radial position inside the particle, mm
R = adsorbent particle radius ($=d_p/2$), mm
R_g = ideal gas constant, kJ/(mol·K)
Sc = Schmidt number ($=\nu/D_l$)
Sh = Sherwood number ($=k_fd_p/D_l$)
t = time, s
T = temperature, K
u = dimensionless solute liquid-phase concentration ($=C/C_o$)
V_f = solution volume, L
W = activated carbon mass, g

Greek letters

α = parameter defined in Eq. 1
α_1, α_2 = Fritz-Schlünder isotherm parameters, (α_1[=] (mg/g) (mg/L)$^{-\beta_1}$, α_2[=] (mg/L)$^{-\beta_2}$)
β_1, β_2 = Fritz-Schlünder isotherm parameters, (β_1, β_2[=] dimensionless)
ΔH_{st} = isosteric heat of adsorption, kJ/mol
$\bar{\epsilon}$ = average power input per unit fluid mass, m^2/min^3
η = dimensionless solute surface concentration ($=q/q_o$)
λ = parameter defined in Eq. 19
ν = fluid kinematic viscosity, mm^2/min
ρ = dimensionless radial position inside the particle ($=r/R$)
ρ_s = apparent particle density, kg/cm^3
τ = dimensionless time ($=D_o t/R^2$)

Subscripts

calc = model-computed value
e = equilibrium value
exp = experimental value
irrev = irreversibly adsorbed
rev = reversibly adsorbed
s = value at solid-liquid interface
sat = value at surface saturation

Literature Cited

Al-Duri, B., and G. McKay, "Prediction of Binary System for Kinetics of Batch Adsorption Using Basic Dyes onto Activated Carbon," *Chem. Eng. Sci.*, **46**, 193 (1991).

Boon-Long, S., C. Laguerie, and J. P. Couderc, "Mass Transfer from Suspended Solids to a Liquid in Agitated Vessels," *Chem. Eng. Sci.*, **33**, 813 (1978).

Brauch, V., and E. U. Schlünder, "The Scale-up of Activated Carbon Columns for Water Purification Based on Results from Batch Tests—II," *Chem. Eng. Sci.*, **30**, 539 (1975).

Brian, P. L. T., H. B. Hales, and T. K. Sherwood, "Transport of Heat and Mass Between Liquids and Spherical Particles in an Agitated Tank," *AIChE J.*, **15**, 727 (1969).

Chozick, R., and R. L. Irvine, "Preliminary Studies on the Granular Activated Carbon-Sequencing Batch Biofilm Reactor," *Environ. Prog.*, **10**, 282 (1991).

Cooney, D. O., A. Nagerl, and A. L. Hines, "Solvent Regeneration of Activated Carbon," *Water Res.*, **17**, 403 (1983).

Crittenden, J. C., D. W. Hand, H. Arora, and B. W. Lykins, Jr., "Design Considerations for GAC Treatment of Organic Chemicals," *J. AWWA*, **79**, 74 (1987).

Famularo, J., J. A. Mueller, and A. S. Pannu, "Prediction of Carbon Column Performance from Pure-Solute Data," *J. Water Pollut. Control Fed.*, **52**, 2019 (1980).

Finlayson, B. A., *Nonlinear Analysis in Chemical Engineering*, McGraw-Hill, New York (1980).

Friedrich, M., A. Seidel, and D. Gelbin, "Kinetics of Adsorption of Phenol and Indole from Aqueous Solutions on Activated Carbons," *Chem. Eng. Process.*, **24**, 33 (1988).

Fritz, W., and E. U. Schlünder, "Simultaneous Adsorption Equilibria of Organic Solutes in Dilute Aqueous Solutions on Activated Carbon," *Chem. Eng. Sci.*, **29**, 1279 (1974).

Fritz, W., and E. U. Schlünder, "Competitive Adsorption of Two Dissolved Organics onto Activated Carbon: I," *Chem. Eng. Sci.*, **36**, 721 (1981).

Fritz, W., W. Merk, and E. U. Schlünder, "Competitive Adsorption of Two Dissolved Organics onto Activated Carbon: II," *Chem. Eng. Sci.*, **36**, 731 (1981).

Furusawa, T., and J. M. Smith, "Intraparticle Mass Transport in Slurries by Dynamic Adsorption Studies," *AIChE J.*, **20**, 88 (1974).

Gilliland, E. R., R. F. Baddour, G. P. Perkinson, and K. J. Sladek, "Diffusion on Surfaces: I. Effect of Concentration on the Diffusivity of Physically Adsorbed Gases," *Ind. Eng. Chem. Fundam.*, **13**, 95 (1974).

Goto, M., N. Hayashi, and S. Goto, "Adsorption and Desorption of Phenol on Anion-Exchange Resin and Activated Carbon," *Environ. Sci. Tech.*, **20**, 463 (1986).

Grant, T. M., and C. J. King, "Mechanism of Irreversible Adsorption of Phenolic Compounds by Activated Carbons," *Ind. Eng. Chem. Res.*, **29**, 264 (1990).

Hand, D. W., J. C. Crittenden, and W. E. Thacker, "User-Oriented Batch Reactor Solutions to the Homogeneous Surface Diffusion Model," *J. Environ. Eng.*, **109**, 82 (1983).

Hutchinson, D. H., and C. W. Robinson, "A Microbial Regeneration Process for Granular Activated Carbon—I. Process Modelling," *Water Res.*, **24**, 1209 (1990).

Itaya, A., Y. Fujita, N. Kato, and K. Okamoto, "Surface Diffusion Coefficient in Aqueous Phases Adsorption on Macroreticular Adsorbents," *J. Chem. Eng. Japan*, **20**, 638 (1987).

Kapoor, A., R. T. Yang, and C. Wong, "Surface Diffusion," *Catal. Rev. Sci. Eng.*, **31**, 129 (1989).

Levins, D. M., and J. R. Glastonbury, "Particle-Liquid Hydrodynamics and Mass Transfer in a Stirred Vessel, Part II—Mass Transfer," *Trans. Inst. Chem. Eng.*, **50**, 132 (1972a).

Levins, D. M., and J. R. Glastonbury, "Application of Kolmogoroff's Theory to Particle-Liquid Mass Transfer in Agitated Vessels," *Chem. Eng. Sci.*, **27**, 537 (1972b).

Mathews, A. P., and I. Zayas, "Particle Size and Shape Effects on Adsorption Rate Parameters," *J. Environ. Eng.*, **115**, 41 (1989).

Mathews, A. P., "Adsorption in an Agitated Slurry of Polydisperse Particles," *AIChE Symp. Ser.*, **230**, 18 (1983).

Mattson, J. S., and H. B. Mark, Jr., *Activated Carbon Surface Chemistry and Adsorption from Solution*, Marcel Dekker Inc., New York (1971).

Mattson, J. S., H. B. Mark, Jr., M. D. Malbin, W. J. Weber, Jr., and J. C. Crittenden, "Surface Chemistry of Activated Carbon: Specific Adsorption of Phenols," *J. Colloid Interface Sci.*, **31**, 116 (1969).

Modell, M., R. deFilippi, and V. Krukonis, "Regeneration of Activated Carbon with Supercritical Carbon Dioxide," in *Activated Carbon Adsorption of Organics from the Aqueous Phase*, Vol. 1, I. H. Suffet and M. J. McGuire, eds., Ann Arbor Science, Ann Arbor, MI (1980).

Muraki, M., Y. Iwashima, and T. Hayakawa, "Rate of Liquid-Phase Adsorption on Activated Carbon in the Stirred Tank," *J. Chem. Eng. Japan*, **15**, 34 (1982).

Neretnieks, I., "Analysis of Some Adsorption Experiments with Activated Carbon," *Chem. Eng. Sci.*, **31**, 1029 (1976).

Nienow, A. W., "The Dispersion of Solids in Liquids," in *Mixing of Liquids by Mechanical Agitation*, Gordon and Breach Science Publishers, New York (1985).

Noll, K. E., V. Gounaris, and W. Hou, *Adsorption Technology for Air and Water Pollution Control*, Lewis Publishers Inc., Chelsea, MI (1992).

Okazaki, M., H. Tamon, and R. Toei, "Interpretation of Surface Flow Phenomenon of Adsorbed Gases by Hopping Model," *AIChE J.*, **27**, 262 (1981).

Peel, R. G., and A. Benedek, "Attainment of Equilibrium in Activated Carbon Isotherm Studies," *Env. Sci. Tech.*, **14**, 66 (1980).

Peel, R. G., A. Benedek, and C. M. Crowe, "A Branched Pore Kinetic Model for Activated Carbon Adsorption," *AIChE J.*, **27**, 26 (1981).

Posey, R. J., and B. R. Kim, "Solvent Regeneration of Dye-Laden Activated Carbon," *J. Water Pollut. Control Fed.*, **59**, 47 (1987).

Radke, C. J., and J. M. Prausnitz, "Adsorption of Organic Solutes from Dilute Aqueous Solutions on Activated Carbon," *Ind. Eng. Chem. Fundam.*, **11**, 445 (1972).

Ranz, W. E., and W. R. Marshall, "Evaporation from Drops. I," *Chem. Eng. Prog.*, **48**, 141 (1952).

Recasens, F., B. J. McCoy, and J. M. Smith, "Desorption Processes: Supercritical Fluid Regeneration of Activated Carbon," *AIChE J.*, **35**, 951 (1989).

Rudling, J., and E. Björkholm, "Irreversibility Effects in Liquid Desorption of Organic Solvents from Activated Carbon," *J. Chromatog.*, **392**, 239 (1987).

Ruthven, D. M., *Principles of Adsorption and Adsorption Processes*, Wiley, New York (1984).

Sano, Y., N. Yamaguchi, and T. Adachi, "Mass Transfer Coefficients for Suspended Particles in Agitated Vessels and Bubble Columns," *J. Chem. Eng. Japan*, **7**, 255 (1974).

Seidel, A., and P. S. Carl, "The Concentration Dependence of Surface Diffusion for Adsorption on Energetically Heterogeneous Adsorbents," *Chem. Eng. Sci.*, **44**, 189 (1989).

Sladek, K. J., E. R. Gilliland, and R. F. Baddour, "Diffusion on Surfaces. II. Correlation of Diffusivities of Physically and Chemically Adsorbed Species," *Ind. Eng. Chem. Fundam.*, **13**, 100 (1974).
Srinivasan, M. P., J. M. Smith, and B. J. McCoy, "Supercritical Fluid Desorption from Activated Carbon," *Chem. Eng. Sci.*, **45**, 1885 (1990).
Sudo, Y., D. M. Misic, and M. Suzuki, "Concentration Dependence of Effective Surface Diffusion Coefficients in Aqueous Phase Adsorption on Activated Carbon," *Chem. Eng. Sci.*, **33**, 1287 (1978).
Suzuki, M., and T. Fujii, "Concentration Dependence of Surface Diffusion Coefficient of Propionic Acid in Activated Carbon Particles," *AIChE J.*, **28**, 380 (1982).
Tan, C., and D. Liou, "Modeling of Desorption at Supercritical Conditions," *AIChE J.*, **35**, 1029 (1989).
Tatterson, G. B., *Fluid Mixing and Gas Dispersion in Agitated Tanks*, McGraw-Hill, New York (1991).
Toth, J., "State Equations of the Solid-Gas Interphase Layers," *Acta Chim. Acad. Sci. Hung.*, **69**, 311 (1971).
Villadsen, J., and M. L. Michelsen, *Solution of Differential Equation Models by Polynomial Approximation*, Prentice-Hall, Englewood Cliffs, NJ (1978).
Yonge, D. R., T. M. Keinath, K. Poznanska, and Z. P. Jiang, "Single-Solute Irreversible Adsorption on Granular Activated Carbon," *Environ. Sci. Tech.*, **19**, 690 (1985).

Manuscript received Dec. 21, 1992, and revision received Apr. 1, 1993.

Statement of Ownership, Management, and Circulation required by 39 U.S.C. 3685 of September 22, 1993, for the *AIChE Journal*, Publication No. 002-580, issued monthly for an annual subscription price of $384.00 from 345 E. 47th St., New York, NY 10017, which is the location of its publication and business offices. The names and addresses of the Publications Director and Editors are: Publications Director, Gary M. Rekstad, 345 E. 47th St., New York, NY 10017; Editor, Dr. Matthew V. Tirrell, Department of Chemical Engineering and Materials Science, University of Minnesota, Minneapolis, MN 55455; and Managing Editor, Haeja L. Han, 345 E. 47th St., New York, NY 10017. The owner is: American Institute of Chemical Engineers, 345 E. 47th St., New York, NY 10017. The known bondholders, mortgagees, and other security holders owning or holding 1% or more of the total amounts of bonds, mortgages, or other securities are: none. The purpose, function, and nonprofit status of this organization and the exempt status for federal income tax purposes have not changed during the preceding 12 months. The following figures describe the nature and extent of *AIChE Journal* circulation. In each category the first number (*in italics*) is the *average number of copies of each issue during the preceding 12 months*. The number next to it, within parentheses ( ), is the actual number of copies of the single issue published nearest to the filing date. Total number of copies printed (net press run), *3,925* (4,000). Paid circulation: 1. sales through dealers and carriers, street vendors, and counter sales, none; 2. mail subscriptions, *2,861* (2,764). Total paid circulation *2,861* (2,764). Free distribution, by mail, carrier, or other means, of samples, complementary, and other free copies: *44* (49). Total distribution: *2,905* (2,813). Copies not distributed: 1. office use, leftover, unaccounted, spoiled after printing, *1,020* (1,187). 2. returns from news agents, none. Total: *3,925* (4,000). I certify that the statements made by me are correct and complete. Gary M. Rekstad, Publications Director.